Supplementary Information (SI) for Inorganic Chemistry Frontiers.

Supporting Information

Optimal Three-Dimensional [$Ag_4P_2S_6$]-Framework Assembly Directed by a Threefold Roto-Inversion Axis for Enhanced Birefringence

Ming-Zhi Zhang [a, b], Chun-Li Hu [a], and Jiang-Gao Mao *, [a]

[a] State Key Laboratory of Functional Crystals and Devices, Fujian Institute of Research on the Structure of Matter, Chinese Academy of Sciences, Fuzhou, 350002, P. R. China.

[b] University of Chinese Academy of Sciences, Beijing 100049, P. R. China.

Corresponding author: Jiang-Gao Mao, E-mail: mjg@fjirsm.ac.cn.

Section S1 Syntheses, Methods, and Reference

Reagents

All the starting materials for synthesis of title compounds (purity higher than 99.9%) were purchased from Beijing Hawk Technology Co., Ltd. and has not been further purified.

Synthesis

Single crystal of γ-$Ag_4P_2S_6$ was prepared via a high-temperature solid-state reaction. In an argon-filled glovebox, a 0.3 g mixture of Ag_2S, P, and S in a molar ratio of 1:2:6 was loaded into a graphite crucible, which was then sealed in an evacuated quartz tube ($\sim 10^{-3}$ Pa) using a hydrogen-oxygen flame. The sealed tube was subsequently heated in a programmable muffle furnace according to a predefined temperature profile. The reaction mixture was heated to 250 °C over 10 h and maintained for 24 h, followed by further heating to 750 °C over 20 h with a dwell time of 120 h. The system was then slowly cooled to 300 °C. After washing with deionized water and ethanol, yellow block-shaped single crystals (Figure S1) were obtained in 60% yield. Notably, compared with the synthesis of the α and β phases, the maximum reaction temperature is reduced by 50 °C.

Methods

Single Crystal X-ray Diffraction

Single-crystal X-ray diffraction data for γ-$Ag_4P_2S_6$ was collected using an Agilent SuperNova dual-wavelength CCD diffractometer with Mo K_α radiation (λ = 0.71073Å). The CrysAlis Pro software package was utilized for data reduction. Numerical absorption corrections based on Gaussian integration over a multifaceted crystal model and empirical absorption corrections using spherical harmonics implemented in SCALE3 ABSPACK scaling algorithm were applied[S1]. The structures were determined by direct method and refined using full-matrix least-squares fitting on F^2 with SHELXL-2017[S2]. PLATON[S3] was used for checking symmetry elements and no higher was given. Crystal data was shown in table S1.

Powder X-ray Diffraction

Powder x-ray diffraction data were collected via a Rigaku MiniFlex600 diffractometer. Scanning was performed with a scan step width of 0.02° using Cu Kα radiation ($\lambda = 1.541886$ Å) in the 2θ range of 10–70°.

Energy-Dispersive X-ray Spectroscopy

Elemental analyses were carried out using a field-emission scanning electron microscope (JSM6700F) outfitted with an Oxford INCA energy-dispersive X-ray spectroscope.

Infrared Spectrum

IR spectra were recorded on a Nicolet Magna 750 Fourier Transform Infrared spectrometer in the spectral range of 4000 to 400 cm^{-1}.

UV-Vis-NIR diffuse reflectance spectroscopy

The Ultraviolet−Visible−Near-IR (UV−Vis−NIR) diffuse reflectance spectrum in the range of 200-2500nm was collected using a PerkinElmer Lambda 950 UV−vis−NIR spectrophotometer, with a barium sulfate powder plate as a 100% reflectance reference. Absorption data is converted from the reflection data by the Kubelka - Munk function $\alpha/S = (1 - R)^2/2R$ (α is the absorption coefficient, S the scattering coefficient, and R the reflectance. The band gap value is the abscissa of the intersection of the absorption edge extension line and the zero absorption.

Raman spectrum

Raman spectra were acquired with a HORIBA HR Evolution spectrometer using a 532 nm laser at 10% power and an exposure time of 15 seconds.

LIDT measurement

LIDT was measured using a 1 Hz 1064 nm Q-switch laser with $AgGaS_2$ as a reference. 150-210 μm particle size sample box was picked out for this test. For a point on the optical element (sample box), increasing pulse energy was raised from 1 mJ until the point is damaged.

Thermogravimetric and differential scanning calorimetry (TG/DSC) analyses

TG/DSC was measured on a NETZCH STA 449F3 thermal analyzer and sample powders were heated under N_2 gas atmosphere from room temperature to 1000 °C at a rate of 10 °C /min.

Birefringence

The birefringence was studied on a polarizing microscope (ZEISS Axio Scope. A1) equipped with a tilting compensator.

Computational Method

Theoretical calculations were performed based on the single crystal structure data of γ-$Ag_4P_2S_6$. The electronic structure and optical properties were analyzed by the plane wave pseudopotential method in the density functional theory (DFT) implemented in the total energy code CASTEP.[S4, S5] For the exchange and correlation functions, we chose Perdew-Burke-Ernzerhof (PBE) in the generalized Gradient Approximation (GGA) [S6]. The interactions between the ionic cores and the electrons were described by the norm-conserving pseudopotential [S7]. The following valence-electron configurations were considered in the computation: Ag $4s^24p^64d^{10}5s^1$, P $3s^23p^3$, S $3s^23p^4$ for γ-$Ag_4P_2S_6$. The numbers of plane waves included in the basis sets were determined by cutoff energies of 765 eV. Monkhorst-Pack k-point samplings of 3×3×4 were used to perform numerical integration of the Brillouin zone. During the optical property calculations, approximately 366 empty bands were involved to ensure the convergence of linear optical properties. The calculations of linear optical properties in terms of the complex dielectric function **$\varepsilon(\omega) = \varepsilon_1(\omega) + i\varepsilon_2(\omega)$** were made. The imaginary part **$\varepsilon_2(\omega)$** can be used to describe the real transitions between occupied and unoccupied electronic states, which was given in the following equation[S8],

$$\varepsilon_2^{ij}(\omega) = \frac{8\pi^2\hbar^2e^2}{m^2V}\sum_k\sum_{cv}(f_c - f_v)\frac{p_{cv}^i(k)p_{vc}^j(k)}{E_{vc}^2}\delta[E_c(k) - E_v(k) - \hbar\omega]$$

The **f_c** and **f_v** represent the Fermi distribution functions of the conduction and valence bands, respectively. The term $p_{cv}^i(k)$ denotes the momentum matrix element transition from the energy level c of the conduction band to the level v of the valence band at a certain k point in the Brillouin zones and **V** is the volume of the unit cell. The **m, e** and **$\hbar$** are the electron mass, charge and Planck's constant, respectively.

Since the dielectric function describes a causal response, the real part **$\varepsilon_1(\omega)$** can be obtained via Kramer-Kronig transform. All optical constants will be derived from the dielectric function **$\varepsilon(\omega)$**, and our main concern, the refractive index **$n(\omega)$** can be expressed as

$$n(\omega) = (1/\sqrt{2})[\sqrt{\varepsilon_1(\omega)^2 + \varepsilon_2(\omega)^2} + \varepsilon_1(\omega)]^{1/2}$$

The polarizability anisotropies of related groups were calculated using the B3LYP/LanL2DZ method with Gaussian 09 software.

Table S1. Summary of Crystallographic data and structure refinements for γ-$Ag_4P_2S_6$.

Formula	$Ag_4P_2S_6$
formula weight	685.78
temperature (K)	293(2)
crystal system	trigonal
space group	$P\overline{3}$ (147)
a (Å)	10.8903(11)
b (Å)	10.8903(11)
c (Å)	7.0537(12)
α (°)	90
β (°)	90
γ (°)	120
V (Å^3)	724.5(2)
Z	3
ρ_{calc} (g/cm^3)	4.716
μ (mm^{-1})	9.546
F(000)	942
λ (Mo Kα) (Å)	0.71073
2θ range for data collection/°	5.78 to 50.00
Index ranges	$-12 \leq h \leq 11$ $-12 \leq k \leq 12$ $-8 \leq l \leq 8$
Rint	0.0609
Goodness-of-fit on F^2	1.278
R1, wR2 [I>2σ (I)][a]	$R_1 = 0.0558$ w$R_2 = 0.1103$
R1, wR2 (all data)	$R_1 = 0.0611$ w$R_2 = 0.1123$
Largest peak/hole (eÅ^{-3})	1.17/−0.83

[a] $R_1 = \Sigma||F_o|-|F_c||/\Sigma|F_o|$; and $wR_2 = \{\Sigma[w(F_o^2-F_c^2)^2]/\Sigma[w(F_o^2)^2]\}^{1/2}$.

Table S2. Atomic coordinates and equivalent isotropic displacement parameters ($Å^2$) for γ-$Ag_4P_2S_6$. U_{eq} is defined as 1/3 of the trace of the orthogonalised U_{ij} tensor.

Atom	x	y	z	Ueq
Ag1	0.73991(15)	0.08820(16)	0.00971(19)	0.0454(5)
Ag2A	0.6575(10)	0.0183(5)	0.5914(11)	0.0431(13)
Ag2B	0.6188(17)	0.0050(13)	0.551(2)	0.0431(13)
P1	0.666667	0.333333	0.4333(8)	0.0129(11)
P2	0.666667	0.333333	0.7553(8)	0.0135(11)
P3	1.000000	0.000000	0.1611(8)	0.0142(12)
S1	0.7593(3)	0.2198(3)	0.3499(5)	0.0202(8)
S2	0.5542(3)	0.1279(3)	0.8322(5)	0.0207(8)
S3	0.7985(3)	−0.0653(4)	0.2416(5)	0.0227(8)

Table S3. Selected bond distances (Å) for γ-$Ag_4P_2S_6$.

Atom–Atom	**Length [Å]**	**Atom–Atom**	**Length [Å]**
Ag1–S1	2.749(3)	Ag2B–S1	2.499(13)
Ag1–S2$^{\#1}$	2.592(4)	Ag2B–S1$^{\#4}$	2.467(13)
Ag1–S3	2.635(4)	Ag2B–S2	2.678(14)
Ag1–S3$^{\#2}$	2.609(4)	P1–S1	2.034(3)
Ag2A–S1$^{\#4}$	2.481(5)	P2–S2	2.015(3)
Ag2A–S1	2.552(6)	P3–S3	2.021(4)
Ag2A–S2	2.630(6)	P1–P2	2.271(8)
Ag2A–S3$^{\#5}$	2.876(11)	P3–P3$^{\#6}$	2.273(11)

Symmetry transformations used to generate equivalent atoms:

#1: +X, +Y, -1+Z; #2: 1+Y, 1-X+Y, -Z; #4: +X, +Y, 1+Z; #5: +X-Y, -1+X, 1-Z; #6: 1+Y, 1-X+Y, 1-Z;

Figure S1. Morphologies of single crystals for γ-$Ag_4P_2S_6$.

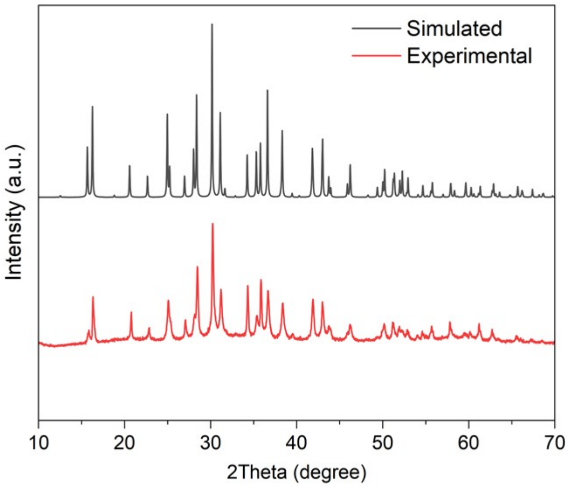

Figure S2. Powder X-ray diffraction patterns (PXRD) for γ-$Ag_4P_2S_6$.

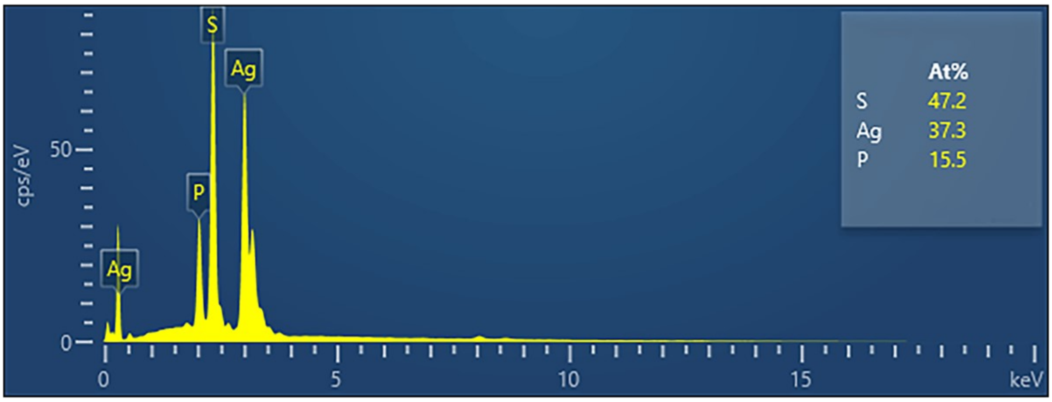

Figure S3. Energy-Dispersive X-ray Spectroscopy (EDS) of γ-$Ag_4P_2S_6$.

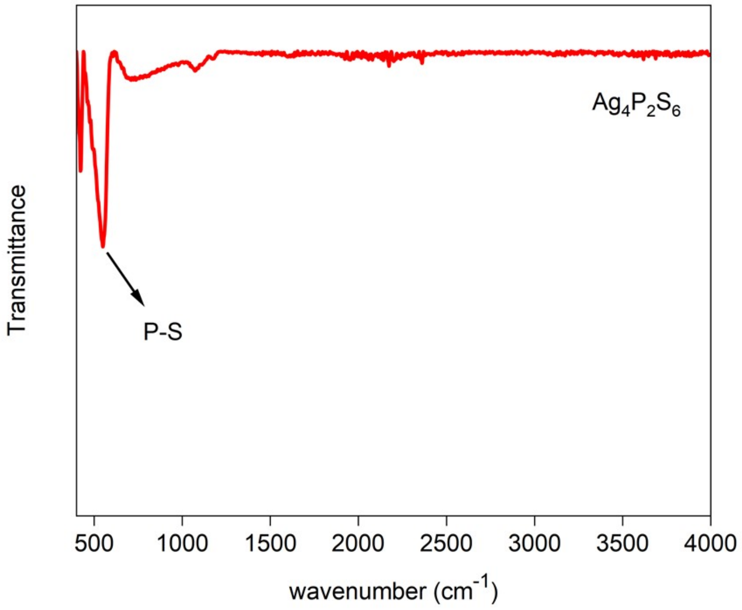

Figure S4. The Infrared (IR) spectrum for γ-$Ag_4P_2S_6$.

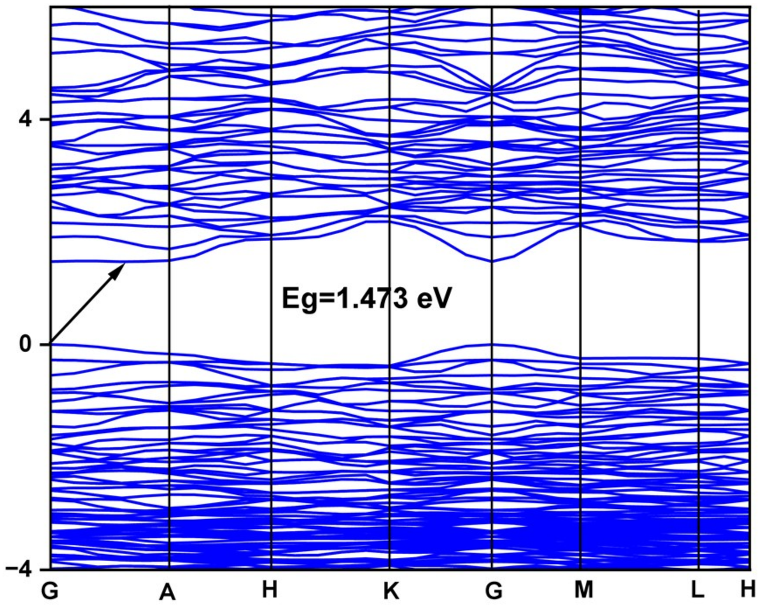

Figure S5. The calculated band structures for γ-$Ag_4P_2S_6$.

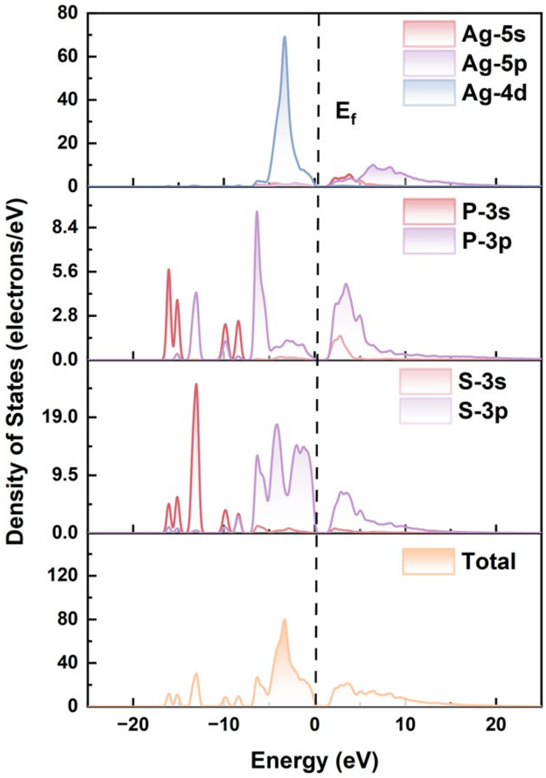

Figure S6. The density of states (DOS) for *γ*-$Ag_4P_2S_6$.

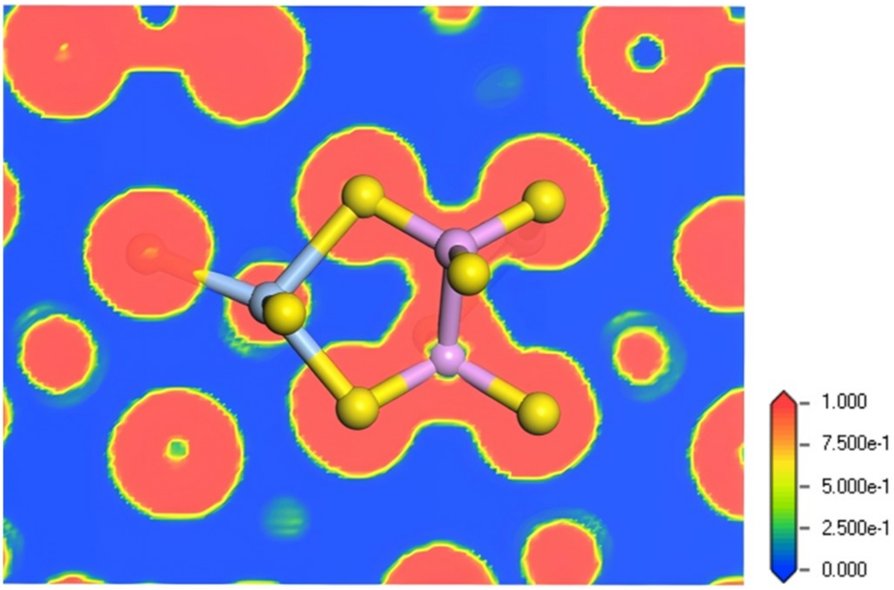

Figure S7. The electron localization function (ELF) graph for *γ*-$Ag_4P_2S_6$.

References

(1) R. Blessing, An empirical correction for absorption anisotropy, Acta Crystallogr. Sect. A, 1995, 51, 33-38..

(2) G. M. Sheldrick, SHELXT - integrated space-group and crystal-structure determination, Acta Crystallogr. A Found. Adv., 2015, 71, 3-8..

(3) A. L. Spek, Single-crystal structure validation with the program PLATON, J. Appl. Crystallogr., 2003, 36, 7-13.

(4) V. Milman, B. Winkler, J. A. White, C. J. Pickard, M. C. Payne, E. V. Akhmatskaya and R. H. Nobes, Electronic structure, properties, and phase stability of inorganic crystals: A pseudopotential plane-wave study, Int. J. Quantum Chem., 2000, 77, 895-910.

(5) M. D. Segall, P. J. D. Lindan, M. J. Probert, C. J. Pickard, P. J. Hasnip, S. J. Clark and M. C. Payne, First-principles simulation: ideas, illustrations and the CASTEP code, J. Phys. Condens. Matter, 2002, 14, 2717-2744.

(6) J. P. Perdew, K. Burke and M. Ernzerhof, Generalized Gradient Approximation Made Simple, Phys. Rev. Lett., 1996, 77, 3865-3868.

(7) J. S. Lin, A. Qteish, M. C. Payne and V. V. Heine, Optimized and transferable nonlocal separable ab initio pseudopotentials, Phys. Rev. B 1993, 47, 4174-4180.

(8) F. Bassani, G. P. Parravicini, R. A. Ballinger and J. L. Birman, Electronic States and Optical Transitions in Solids, *Phys. Today*, 1976, **29**, 58-59.